TR-AC-0006 015

Molecular Beam Epitaxy Growth on GaAs(n11)A Substrates and Device Applications

藤田　和久

1997. 6.27

ATR環境適応通信研究所

Molecular beam epitaxy growth on GaAs (n11)A substrates and device applications

Kazuhisa Fujita

ATR Adaptive Communications Research Laboratories, 2-2
Hikaridai, Seika-cho, Soraku-gun, Kyoto 619-02, Japan

Contents

Abstract	1
1. Introduction	2
2. MBE growth	3
2.1. Pre-growth treatment	3
2.2. GaAs growth	3
2.3. AlGaAs growth	5
2.4. InGaAs growth	6
3. Growth on patterned substrate	8
3.1. Carrier confinement structure	8
3.2. Lateral tunneling devices	9
4. Nanostructures	10
5. Conclusion	12
Acknowledgements	14

Abstract

Gallium Arsenide (GaAs) is widely used as a material for fabricating devices such as high mobility transistors and laser diodes. Studies on the growth of GaAs layers have mainly been carried out using GaAs(100) substrates due to the maturity of (100) substrate technology. However, it has been reported that GaAs layers grown on GaAs(n11)A (n≤3) substrates have many advantages such as the amphoteric nature of a Si dopant, a high emission efficiency and the piezoelectric effect.

In this article, I review techniques for growth on GaAs(n11)A substrates and properties of epitaxial layers. Furthermore, I also review applications to devices such as tunneling transistors and laser diodes.

Keywords: Molecular beam epitaxy; GaAs(111)A; Si-doping; Piezoelectric effect; Nanostructure

1. Introduction

III-V compound semiconductors traditionally have been grown on (100) oriented substrates because high-quality epitaxial layers can be grown under a wide range of growth conditions by molecular beam epitaxy (MBE). Recently, however, there has been great interest in the growth of III-V compound semiconductors on substrates other than (100).[1] This interest can be attributed to the great potential these semiconductors have for fabricating low-threshold laser diodes,[2,3] piezoelectric devices,[4] novel carrier confinement structures[5,6] and lateral p-n junction formations.[7,8] More specifically, the fundamental material properties of non-(100) faces include a high emission efficiency, the piezoelectric effect caused by strained layer growth, and the amphoteric nature of a Si dopant; in GaAs growth on GaAs(n11)A substrates, Si atoms are incorporated as acceptors when $n \leq 3$.[9-12]

The {111} surface is of particular importance because, for example, GaAs(100) patterned substrates with a {111} surface are frequently used in fabricating quantum wires and dots. In addition, it has been predicted that large polarization fields can be generated by the piezoelectric effect in strained-layer heterostructures grown on (111) surfaces.[4] Furthermore, quantum wells (QWs) grown on a {111} surface have an enhanced radiative transition rate, which in turn has led to the development of a low-threshold (111)B QW laser.[2] This laser was obtained by layer growth on a GaAs(111)B surface because it has become practical to grow GaAs and AlGaAs layers with good surface morphologies on (111)B substrates. On the other hand, the growth of high-quality GaAs, AlGaAs and InGaAs on GaAs(111)A is itself still a subject of research.[13-15]

We have systematically investigated crystal growth and impurity doping characteristics on GaAs(111)A substrates by using MBE and through device applications. It has been found in the course of the research that the techniques developed for epitaxial growth on (100) substrates are not directly applicable to (111)A substrates because of the difference in the surface chemical and electronic properties resulting from the different surface atomic configurations. We have recently reported MBE-grown GaAs layers with excellent surface morphologies by developing a pre-growth treatment. Also, we have reported a lateral tunneling transistor on a patterned (111)A substrate by a plane-dependent Si-doping technique and a polarization controlled surface emitting laser diode on a (311)A substrate.

In this article, I review techniques for growth on GaAs(n11)A substrates and properties of epitaxial layers grown on the substrates. I also review applications to devices such as tunneling transistors and laser diodes. Finally, I report quantum structures formed on (n11)A substrates.

2. MBE growth

2.1. Pre-growth treatment

The surface morphology of a GaAs growth layer on exactly oriented GaAs(111)A is strongly dependent on the stoichiometry and roughness of the surface before growth. To obtain a GaAs layer with a good surface morphology, the surface profiles before GaAs growth must be controlled. H_2SO_4 solutions is widely used as an etchant for GaAs(100) substrates. However, it is difficult to get an atomically flat (111)A surface by using this etchant. Figure 1 shows etching processes for (111)A wafers and SEM photographs of the surface morphologies of 1-μm Si-doped GaAs layers grown on the substrates.[16] The layers were grown by an MBE Varian Modular Gen II. A mirror-like surface could be observed for a sample with the A-type process [Fig. 1(A)]. On the other surfaces, two kinds of defects could be observed: three pyramids having a (100)-related surface for (D)-(F) and a single pyramid with a (110)-related surface for (B)-(F). These defects are related to surface profiles formed by etching, depending on the etching rates of all the etchants for (100) and (110) surfaces. Only the A-type etchant can cause slow etching for (111)A surfaces and less selective etching for (100) and (110) surfaces. From these results, the etchant used in the A-type process is suitable for etching (111)A surfaces. Another important factor for obtaining device-quality layers with a good surface morphology is reducing the residual As_4 pressure at wafer loading into an MBE chamber; the formation of defects such as triplet pyramids results from an As-rich environment on the GaAs surface before MBE growth.[16]

Since a GaAs(111)A substrate has only Ga atoms on the surface, the surface state density can be decreased by growing a GaAs layer on a clean (111)A surface. It was reported that the surface state density of an n-type epilayer on a GaAs(111)A substrate is lower than that on a GaAs(100) or (110) substrate.[17] This fact opens the door for achieving metal-insulator-semiconductor (MIS) structures on GaAs substrates by using (111)A oriented substrates.

2.2. GaAs growth

Silicon is widely used as an n-type dopant in GaAs growth using MBE. However, it has been reported that in GaAs growth on GaAs(n11)A substrates, Si atoms are incorporated as acceptors when $n \leq 3$.[9-12] Furthermore, Si can be highly doped as a p-type dopant. Figure 2 shows free carrier concentrations at room temperature of Si-doped GaAs as a function of [Si].[18] The hole concentration of (111)A films correspondingly increases with [Si] up to about 6×10^{19} cm^{-3}. It should be noted that the doping characteristics of (111)B growth have a strong resemblance to those of (100) growth.

Due to the unique bonding structure on a GaAs(n11)A surface, the conduction type of a Si-doped layer for GaAs growth on GaAs(n11)A ($n \leq 3$) can be controlled by the growth conditions such as the V/III flux ratio and the off-angle for a misoriented substrate.[12,19,20] Figure 3 shows the conductivity map in plane of tilting angle (φ) of a misoriented substrate and flux ratio (γ).[12] Here, n-type conductivity appears at a large off-angle and a high flux ratio. The conductivity dependence on the off-angle can be explained as follows: The misorientation of a (111)A substrate toward a (100) orientation induces a large number of surface steps with a (100)-like bonding geometry as shown in Fig. 4;[21] the (100) step can promote the decomposition of As_4 molecules and induces lateral growth from the steps leading to a (100)-like incorporation of the Si, i.e., n-type conductivity. Therefore, the conductivity type is determined by the competition of Si incorporation for (111)A terrace sites and (100) step sites. As the off-angle is increased, the (100)-step density increases, resulting in n-type conductivity.

The dotted line in Fig. 3 shows the amounts and occupation sites of incorporated Si treated independently for both (100) and (111)A surface bonds under the neutral condition of $N_D=N_A$. Note that the surface morphology of the GaAs layer grown improves for off-angles above 5° due to the step-flow growth mode.

The conductivity type dependence on the flux ratio can be explained as follows: since a GaAs(111)A surface has only Ga atoms, almost all of the Si atoms occupy As sites and act as acceptors when the flux ratio is low. However, by increasing the ratio, it becomes difficult for the Si atoms to occupy As sites and instead results they occupy Ga sites. Therefore, the conductivity type is determined by the competition of Si and As for As sites.

All Si atoms occupy As sites substantially in Si-doped GaAs layers grown on exactly GaAs(111)A, and are thermally stable.[22-24] Figure 5 shows SIMS depth profiles (a) for Si at a Si delta-doped GaAs layer and (b) for Be at a Be delta-doped GaAs layer.[22] The samples were annealed at 850°C for 30 s. As shown in Fig. 5(a), the Si profile is still sharp after annealing. By contrast, the Be profile becomes broader after annealing, as shown in Fig. 5(b). This indicates that Si is more stable as a p-type dopant on exactly (111)A GaAs when compared to Be. There is a strong correlation between the step density and the diffusion coefficient. GaAs(111)A substrates misoriented in the [001] direction and [110] direction induce the (001) step and the (110) step, respectively. Figure 6 shows the diffusion coefficient for Si and the step density versus off-angle of a misoriented GaAs(111)A substrate.[25] The diffusion coefficient was calculated by means of the following approximation:[26]

$$Z_d^2 = 2D_{Si}\,t = (FWHM_A^2 - FWHM_0^2) / 4. \quad (1)$$

Here, Z_d is the diffusion distance, D_{Si} is the one-dimensional diffusivity, and t is the anneal time. $FWHM_A$ and $FWHM_0$ denote the FWHM of the Si profile for an annealed sample and

an as-grown sample, respectively. The step density is calculated as 1/L using the terrace length (L) shown in Fig. 6. The diffusion coefficient for exactly (111)A is the smallest, and becomes larger as the off-angle increases in the [110] or [001] direction. The diffusivity of Si is proportional to the step density, indicating a step-related diffusion. Note that the diffusion coefficient decreases above (331) and (113)A. Sakamoto et al.[27)] reported that the mechanism for the conduction-type conversion in Si-doped (113)A GaAs differs from that for the (111)A orientation. This suggests that the diffusion for (113)A is caused by a different mechanism that that for the (111)A orientation.

2.3. AlGaAs growth

The surface morphology and the conduction type of Si-doped AlGaAs layers were also affected by the off-angle of misoriented GaAs(111)A substrates. Figure 7 shows 1-μm Si-doped AlGaAs layers grown on (111)A substrates misoriented toward the [001] direction;[28)] the surface morphology is drastically improved when the off-angle is over 5°. Figure 8 shows the dependence of the carrier concentration of Si-doped AlGaAs on the off-angle of substrate orientation at several flux ratios.[28)] When the flux ratio is 2, the conductivity is p-type; at the off-angle of 5°, the hole concentration agrees with the incorporated Si concentration, indicating that all of the Si atoms substantially occupy As sites. As the off-angle increases, the hole concentration decreases. On the other hand, some Si atoms occupy Ga sites at flux ratios above 5, indicating n-type conductivity. The concentration increases with increasing off-angle because of an increase in the number of steps leading to the (100)-like incorporation of Si. These results indicate that the off-angle of GaAs(111)A substrates is an important factor for improving the surface morphology and controlling the impurity concentration of AlGaAs layers.

As for n-type AlGaAs layer grown, the electron concentration was below the incorporated Si concentration due to compensation, which was ascribed to donor-acceptor (DA) pair recombination, as shown in Fig. 8. To improve the quality of an n-type AlGaAs layer, a group VI element such as selenium (Se) can be effectively used as a dopant because the Se donor has a lower DX center concentration than Si.[29)] It has been reported that the thermal activation energies for carrier release and capture for a Se-related DX center are lower than those for a Si-related DX center.[30)] From the results of isothermal capacitance transient spectroscopy experiments under pressure, the coexistence of two deep donor states with and without capture was observed for a Se-doped $Al_xGa_{1-x}As$ layer on a (111)A substrate.[31)]

The conductivity type of Si-doped GaAs and AlGaAs layers grown on GaAs(n11)A can

be controlled by controlling the growth conditions. By using this technique, Li et al.[32] demonstrated all-Si doping n-p-n GaAs/AlGaAs heterojunction bipolar transistors on GaAs(311)A substrates. For our part, we demonstrated GaAs p-n junction LEDs[22, 33] and AlGaAs/GaAs double-heterostructure LEDs[34,35] on GaAs(111)A and (211)A substrates. These LEDs with all-Si doping have a better device quality because Si as the p-type dopant is more temperature stable than Be as the p-type dopant. The (311)A face has a (100)-like stable growth mode, which leads to a good growth morphology and a high-quality material. Henini et al.[36] reported Si-doped GaAs/(AlGa)As two-dimensional hole gas structures with very high mobilities on (311)A GaAs surfaces.

High-quality AlGaAs and InGaAs single quantum wells (SQWs) are basically required for the successful fabrication of devices. We have grown AlGaAs/GaAs single quantum wells with a heterointerface roughness of less than one monolayer on exactly and (111)A substrates misoriented 5°toward [100].[37] This was based on improved surface morphologies by growing on misoriented substrates. However, when the off-angle of misoriented substrates is small, growth on (111)A terraces becomes dominant, and this causes periodic lateral structures of Al content modulations in AlGaAs for 3°-misoriented (111)A samples; numerous giant terraces have steps faced not in the off-angle of the [100] direction but in the [101] and [110] directions.[38] These novel lateral structures are most likely caused by the different sticking coefficients of Ga adatoms on (111)A surfaces and (110) surfaces.

Crystal structures of Si-doped AlAs layers grown on (111)A were found to be strongly dependent on substrate misorientations; hexagonal AlAs was grown on exactly oriented (111)A and zincblende AlAs was grown on misoriented (111)A.[39] Si-doped AlAs with a zincblende structure showed n-type conductivity and low resistivity, and that with a hexagonal structure exhibited high resistivity ($>10^5$ Ω·cm). Therefore, for applying AlAs/GaAs multiple quantum wells (MQWs) to a distributed Braggs reflector (DBR) on exactly oriented (111)A, a slightly misoriented substrate must be used. All of the surface defects in the DBRs on the misoriented substrate can be completely eliminated by introducing In into the AlAs layer.[40]

2.4. InGaAs growth

Polarization fields are generated by the piezoelectric effect in strained-layer SQWs grown on GaAs(n11) surfaces. Growth of strained InGaAs on GaAs(111)A is quite difficult. The epilayers show strain relaxation by formation of dislocations. Figure 9 shows the

photoluminescence peak energy dependence on the well thickness for SQWs on (111)A substrates.[41] The SQWs were grown on semi-insulating GaAs substrates with the following orientations: (100), exactly oriented (111)A, and (111)A misoriented 1° and 5° toward [001] and [110]. Each grown structure consisted of a 200 nm GaAs buffer layer, three $In_{0.18}Ga_{0.82}As$ SQWs 10, 5 and 2.5 nm thick separated by 50 nm GaAs barriers, and a 50 nm cap layer. The InGaAs layers were biaxially compressed in the plane of the SQWs. The strain increased the band gap and shifted the band alignment at the heterointerfaces. The strained bandgap was calculated using the model of Pollak;[42] the band alignment was calculated using the solid model of Van de Walle[43] for (100) and (111)A surfaces.

The strained InGaAs layers grown on the (111)A oriented substrates had a built-in electric field due to the piezoelectric effect. This electric field was normal to the plane of the SQWs and it produced a tilt of the band edges inside the SQWs. For x=0.18 in the (111) direction, the electric field calculated using the bulk piezoelectric theory was E=257 kV/cm.[44]

The long-dashed line in Fig.9 shows the calculated transition energies for the SQWs including this electric field. QWs grown on just oriented and 1° off substrates show PL peaks at an energy lower than the expected from theory. This behavior is attributed to partial strain relaxation. The PL peak of the QWs grown on GaAs(111)A 5° off [100] agree with a piezoelectric field of 154 kV/cm. An interface charge density at the heterointerfaces could have been responsible for the observed reduction in the built-in electric field.[45] Since the samples grown on the GaAs(111)A substrates 5°off toward [001] showed the best optical characteristics, this substrate orientation was chosen for making p-i-n diodes.[46] The PL peak corresponding to a 10 nm SQW blue shift was as much as 24 meV with only 1.2 applied reverse bias. The large blueshift of the PL peak energy under moderated illumination intensity suggests the possibilities of application for optical bistable devices. These devices need an external bias when they are grown on GaAs(100) substrates to obtain a redshift of the excitonic absorption peak. This kind of device grown on a GaAs(111)A substrate requires no external bias and can be operated without the need for electrical contact.

The (111)A sample shows the largest PL peak red shift because it has the stronger piezoelectric field. Figure10 shows the time dependence of the PL peak wavelength for InGaAs SQWs grown on (111)A, (211)A and (311)A substrates.[47] The piezoelectric field for the SQWs grown on the (311)A substrate is smaller than that on the (111)A substrate. However, this field is strong enough for application in some devices.

The radiative recombination rate is enhanced in (311)-oriented InGaAs/GaAs quantum well structures in comparison to (100)-oriented ones. We have reported graded-index sepa-

rate-confinement heterostructure double quantum-well lasers on (311)A having a low threshold current density of 360 A/cm^2 for a 1.17 mm long laser at room temperature.[48] The piezoelectric effect does not seem to affect adversely the laser operation.

It has theoretically been predicted that the band structure of strained-layer (SL) QWs can be modified by substrate orientation, and that SL-QWs grown on non-(100) substrates have a high and anisotropic optical gain.[49,50] Kaneko et al. reported an InGaAs/GaAs vertical-cavity surface-emitting laser (VCSEL) on a (311)B substrate having an anisotropic gain.[51] We reported an InGaAs/GaAs VCSEL on a GaAs(311)A substrate showing a low threshold and stable polarization.[52]

Figure11 shows light output power versus polarizer angle at 1.5 times the threshold. The extinction ratio between orthogonal polarization states was 9.8 dB, which corresponds to a net gain difference of 5% between two polarization modes. In the figure, a [$\bar{2}$33] polarization mode is stable against the injection current of 3 times the threshold. Furthermore, a threshold current density of 80 A/(cm^2·well) is achieved for a device with a laser aperture of as large as 25μm square, which is comparable to or even lower than that of (100)-oriented VCSELs.

3. Growth on patterned substrate

3.1. Carrier confinement structure

A GaAs(111)A surface was prepared by etching to have a three-fold symmetry, and therefore an equilateral triangle pattern, in which the three sidewalls had equivalent crystallographic faces. As a result, a lateral carrier confinement structure could be obtained by a single-step MBE growth process, i.e., the growth of an Si-doped GaAs layer on a patterned (111)A substrate. However, applying this technique to the formation of a carrier confinement structure requires the suppression of all extra facets generated on the sidewall, because they act as leakage paths.

It has been reported that the intersection angle φ of a sidewall to a (111)A substrate plane, affects the generation of extra facets at the corners of the triangles. The formation of extra facets is strongly related to the Ga migration length during MBE growth.[53] An investigation into local variations in the layer thickness in regions adjacent to those facets common to (111)A and (001) patterned substrates, and to extra facets specific to the respective substrates, together with an investigation on the the relative growth rates of the facets, found that the orientation-dependent Ga surface diffusion length λ_{Ga} is as follows: $\lambda_{Ga}(001) \approx \lambda_{Ga}(\bar{1}\bar{1}\bar{3})B < \{\lambda_{Ga}(\bar{1}\bar{1}\bar{1})B, \lambda_{Ga}(\bar{3}\bar{3}\bar{1})B, \lambda_{Ga}(013), \lambda_{Ga}(113)A\} < \lambda_{Ga}(159) \approx \lambda_{Ga}(114)A \approx \lambda_{Ga}(111)A < \lambda_{Ga}(110)$, and that it is possible to grow a GaAs layer without extra facets in the

narrow ϕ range of 28° to 33°.[54] Therefore, we chose 29.5° as the sidewall orientation, which corresponds to a (311)A surface, to achieve a confinement structure. The intersection angle was controlled in the range of 84° to 11° using $HF+H_2O_2+H_2O$ mixtures of various compositions.[55]

Figure 13 shows the SEM image of a 1-μm Si-doped GaAs layer grown on a patterned GaAs(111)A substrate with (311)A sidewalls. The surface morphology is very smooth and extra facets can not be observed at the corners of the triangles.[56] The size of the triangular (111)A region was reduced by reducing the size of the photoresist pattern. Figure 14 shows CL images of the sample with a submicron ridge-type triangle. In the figure, the p-type triangular (111)A region is fully isolated from the n-type (311)A sidewall regions. The peak wavelength of the triangular region is 836 nm and that of the sidewall is 823 nm. These wavelengths correspond to those in the CL spectra of the Si-doped GaAs layer, whose conduction types were confirmed by Hall measurement. This finding indicates that a lateral carrier confinement structure is formed on the patterned (111)A substrate. The pattern size will be further reduced to the nanometer scale by using a fabrication technique such as electron beam lithography. The confinement structure was also confirmed by an investigation on its current-voltage characteristics[57] and electroluminescence from the lateral p-n junction.[58]

3.2. Lateral tunneling devices

Negative differential resistance (NDR) devices based on tunneling[59] have attracted much interest because of their potential for high-speed, low-power and multi-functional device applications. A new three-terminal tunnel device, the surface tunnel transistor, was proposed[60] and demonstrated to have an NDR due to interband tunneling at room temperature.[61] The device was fabricated through the regrowth of GaAs/AlGaAs on a mesa-type $p^+/i/n^+$ GaAs diode on a GaAs(100) substrate. We have reported an NDR due to interband tunneling by using a lateral p-n junction formed on a patterned GaAs(111)A substrate with (311)A sidewalls.[62] In this case, the δ-doping technique was adopted to obtain an abrupt p-n junction. Also, a novel carrier confinement structure with lateral p-n subband junctions was obtained by growing a Si δ-doped AlGaAs/GaAs multiple quantum well structure on the patterned (111)A substrate.[63]

The Si δ-doping technique is effective for achieving an abrupt p-n junction for GaAs grown on a patterned (111)A substrate. However, it is difficult to apply this structure to a transistor due to a low current density in the lateral p-n junction. Recently, we have suc-

ceeded in developing lateral interband tunneling transistors by using uniformly Si-doped GaAs layers grown on a patterned (111)A substrate with (511)A sidewalls and on a patterned GaAs(311)A substrate with (100) sidewalls.[64] In these structures, the interband tunneling phenomenon was observed between the p-type layer on the top surface and the n-type layer on the extra (411)A facet formed on top of the sidewalls. It should be noted that extra (411)A facets, which must be suppressed for carrier confinement structures, play an important role for the formation of an abrupt p-n junction.

The transistors exhibited gate-controlled NDR characteristics in the forward drain bias region. Figure 15 shows a schematic cross-sectional view of a transistor on a patterned (411)A substrate.[65] An abrupt p-n junction was formed between the n-type (411)A surface and an extra (311)A facet at the top corner of the (211)A sidewall. In this case, the facet had p-type conductivity. Figure 16 shows drain current-voltage characteristics of the transistor at room temperature (RT). The drain voltage is swept from 0.0 to 0.5V with the gate voltage applied in steps of 3.0 V from -1.5 to 4.5 V. In the figure, gate-controlled NDR characteristics due to interband tunneling are clearly observed even at RT. These results indicate that the tunneling current is controlled through modulation of both the carrier concentration and the tunneling barrier width by changing of the gate voltage.

The lateral tunneling devices were successfully fabricated on a patterned (n11)A substrate by using a plane-dependent Si-doping technique. This technique provides a simpler process for the fabrication of tunneling transistors.

4. Nanostructures

A number of reports have been made on achieving quantum structures by using patterned substrates.[66-69] Recently, a new and promising fabrication method has been presented,[70, 71] where $In_xGa_{1-x}As$ with a high indium concentration grows bidimensionally by using MBE or metalorganic chemical vapor deposition (MOCVD) on a GaAs substrate until reaching a certain critical thickness where it transforms to a three-dimensional surface. This surface consists of small $In_{0.5}Ga_{0.5}As$ dots about 20 nm in diameter and 4 nm in height. These dots are formed because the highly strained epilayer decreases its energy by the formation of islands after layer-by-layer growth, in the Stranski-Krastanow growth mode.[72-74]

Most of the current research focuses on GaAs(100)-oriented substrates, but a report is also available on $In_{0.5}Ga_{0.5}As$ quantum dots grown by MOCVD on 0° and 41° toward (111)B[75] and another report uses GaAs(311)B-oriented substrates.[76] Moreover, corrugated surfaces of strained $In_xGa_{1-x}As$ grown on GaAs and InP(311)A-oriented substrates by MBE have

been obtained.[77)]

The photoluminescence spectrum of a sample on GaAs(311)A where the $In_{0.5}Ga_{0.5}As$ nanostructure was covered with a GaAs cap layer, showed a strong peak up to room temperature.[78)] Figure 17 shows the radiative recombination time constant dependence on temperature for nanostructures and conventional quantum wells grown on (311)A and (100) substrates. Data for conventional quantum wells (closed symbols) are taken from ref. 52, where the difference between (311)A and (100) radiative recombination times is explained. These conventional quantum wells show the usual increase of radiative recombination time with temperature.[79)] Excitons are thermally excited to higher states where radiative recombination is not allowed because of momentum conservation, therefore only a small fraction of excitons which have lower momentum can recombine radiatively as temperature increases. On the other hand, the (100) sample which has quantum dots show very little increase of radiative recombination time with temperature. This behaviour shows that there are not states where excitons can be thermally excited in this temperature range, i. e., there is a gap in the density of states of the quantum dots between the fundamental level and the excited levels as predicted by theory. Besides, the short radiative recombination time (less than 1 ns up to 140 K) is very promising for application in light emitting devices. The (311)A sample with corrugated nanostructure also shows little increase in radiative recombination time up to 100 K, indicating the presence of a gap in the density of states. The steep increase for higher temperatures shows that excitons are excited to states with higher momentum from where radiative recombination is not allowed. We estimate from the exponential increase of the radiative recombination time that the energy gap between the fundamental and the first excited level is less than 10 meV. The experimental temperature dependence of the radiative recombination time for the corrugated sample is similar to that expected for quantum dots, and it does not agree with the dependence predicted theoretically for quantum wires.[79)] The radiative recombination time for quantum wires should show a fast increase at low temperatures and a slower increase at higher temperatures. Therefore we suppose that excitons are localized in the thicker regions of the wire-like structure at low temperature and they become excited to non-localized states as temperature increases above 100 K. This view is supported also by the radiative time constant (less than 10 meV). This nanostructure is a good example of how structures with an arbitary topology may have better optical properties than quantum dots grown under the same conditions.

InAs epilayers grown on substrates with other orientations also showed the formation of interesting nanostructures. Figure 18 shows the morphology of a GaAs buffer layer and surfaces after an amount of InAs equivalent to zero, one, two and three monolayers was deposited on GaAs(411)A, exactly (111)A, and 15° off-oriented substrates, observed by AFM.[80)]

Each micrograph shows an area of 1 μm x 1 μm. The horizontal direction in the micrographs corresponds to the $(0\bar{1}1)$ direction, and the vertical direction corresponds to the $(\bar{2}11)$ direction. The (411)A sample shows a very flat surface with streaks due to the particular surface reconstruction.[81)] The formation of InAs nanostructures on the (111)A-oriented substrate is strongly influenced by the buffer layer's morphology. The successive InAs layers produce a net effect of planarization of the surface. This result is in agreement with the recent RHEED measurements of Yamaguchi et al.,[82)] where they show that InAs grows in a two-dimensional mode, without the formation of three-dimensional islands unlike in the Stranski-Krastanow growth mode.

The most promising nanostructures obtained are those grown on (111)A-15° off-oriented substrates. The densely packed dot structures are expected to show the effect of overlap of the wave function for carriers in adjacent dots, with consequences for the inplane transport properties of the dot layer. In the case of application to light-emitting devices, the high inplane tunneling probability would allow the fast relaxation of excitons toward the lower energy regions, narrowing the emission line width. These results show that the growth of strained epilayers on non-(100)-oriented substrates is a promising method for developing new low-dimensional nanostructures. Moreover, this study on the early stage of epitaxy on non-(100)-oriented substrates provides insight into the fundamental growth mechanism.

5. Conclusion

As a pre-growth treatment for an exactly oriented GaAs(111)A surface, NH_4OH etchants ($NH_4OH:H_2O_2:H_2O$ = 2:1:96) are suitable, and wafer loading into an MBE growth chamber under a small residual As_4 pressure is necessary for achieving device-quality layers with a good surface morphology.

In GaAs growth on GaAs(n11)A substrates, Si atoms were incorporated as acceptors when $n \leq 3$. Moreover, Si was highly doped as a p-type dopant up to about 6×10^{19} cm^{-3} in GaAs layers grown on a (111)A substrate. Si was more stable as a p-type dopant on GaAs(111)A when compared to Be. There was a strong correlation between the step density and the diffusion coefficient; the diffusivity of Si was proportional to the step density, indicating step related diffusion. The conduction type of Si-doped GaAs and AlGaAs layers on the (n11)A substrate was controlled by the growth conditions such as the V/III flux ratio and the off-angle of the misoriented (111)A substrate. By using this technique, AlGaAs/GaAs double-heterostructure LEDs were fabricated on (111)A substrates by using only Si dopant.

The surface morphology of GaAs (AlGaAs) was strongly affected by the off-angle of misoriented (111)A substrates; a mirror surface was obtained when the off-angle was over 5°toward the [001] direction. Crystal structures of Si-doped AlAs layers grown on the (111)A substrates were also affected by the substrate misorientations; hexagonal AlAs was grown on

exactly oriented (111)A and zincblende AlAs was grown on misoriented (111)A.

InGaAs/GaAs SQWs grown on GaAs(111)A substrates showed the largest PL peak red shift due to a stronger piezoelectric field. The piezoelectric field for SQWs grown on a (311)A substrate was smaller than that on the (111)A substrate. Note, however,that this field is strong enough for application in some devices. The radiative recombination rate was enhanced in (311)-oriented InGaAs/GaAs quantum well structures compared to (100)-oriented ones. Also, a InGaAs/GaAs vertical-cavity surface-emitting laser grown on a GaAs(311)A substrate showed a low threshold and stable polarization.

A lateral carrier confinement structure was fabricated on a patterned (111)A substrate with (311)A sidewalls by a single-step MBE growth process of an Si-doped GaAs layer. Furthermore, by using a lateral p-n junction formed on the patterned substrate, a lateral tunneling transistor was demonstrated. Gate-controlled negative differential resistance characteristics were observed in the forward drain bias region. They were due to an abrupt p-n junction formed between the top surface and an extra facet at the top corner of the sidewall.

Small $In_{0.5}Ga_{0.5}As$ dots were formed on GaAs(n11) substrates by utilizing the Stranski-Krastanow growth mode. The most promising nanostructures obtained were those grown on (111)A-15° off-oriented substrates. The densely packed dot structure can be expected to show the effect of overlap of the wave function for carriers in adjacent dots, with consequences for the in-plane transport properties of the dot layer.

We have reviewed techniques for growth on GaAs(n11)A substrates, properties of epitaxial layers and applications to devices such as tunneling transistors and laser diodes. We also reported the formation of nanostructures on (n11)A substrates. We hope that this article provides useful imformation for all researchers who plan to start studies concerning epitaxial growth on non-GaAs(100) substrates.

Acknowledgements

Most of the study was carried out at ATR Optical and Radio Communications Research Laboratories. The author would like to thank Drs. Y. Furuhama, H. Inomata and B. Komiyama for their encouragement throughout this work.

The author would also like to thank Drs. I. Fujimoto, K. Kobayashi, T. Watanabe, N. Egami and Pablo O Vaccaro for valuable discussions, and all researchers who joined this ATR project. Their names are shown in the referenced papers; Drs. Y. Okano, M. Shigeta, T. Takebe, T. Yamamoto, M. Takahashi, H. Ohnishi, M. Fujii, D. R. Lovell, M. Inai, A. Shinoda, M. Hirai and K. Nitatori, and co-authors.

References

1) as a recent review, see, for example, S. Hiyamizu, Y. Shiraki and S. Gonda: J. Cryst. Growth 150 (1995); M. Henini: Microelectronics J. 26 (1995).
2) T. Hayakawa, M. Kond, T. Suyama, K. Takahashi, S. Yamamoto and T. Hijikata: Jpn. J. Appl. Phys. 26 (1987) L302; T. Hayakawa, T. Suyama, K. Takahashi, M. Kondo, S. Yamamoto and T. Hijikata: Appl. Phys. Lett. 52 (1988) 339.
3) A. T. Meney: Supelatt. and Microstruc. 11 (1992) 387.
4) D. L. Smith: Solid State Commun. 57 (1986) 919; D. L. Smith and C. Mailhiot: Phys. Rev. Lett. 58 (1987) 1264; C. Mailhiot and D. L. Smith: Phys. Rev. B35 (1987) 1242.
5) A. Madhukar, K. C. Rajkumar and P. Chen: Appl. Phys. Lett. 62 (1993) 1547; K. C. Rajkumar, A. Madhukar, P. Chen, A. Konkar, L. Chen L, K. Rammohan and D. H. Rich: J. Vac. Sci. & Technol. B12 (1994) 1071.
6) M. Fujii, T. Yamamoto, M. Shigeta, T. Takebe, K. Kobayashi, S. Hiyamizu and I. Fujimoto: Surf. Sci. 267 (1992) 26.
7) D. L. Miller: Appl. Phys. Lett. 47 (1985) 1309.
8) H. P. Meier, R. F. Broom, P. W. Epperlein, E. van Gieson , Ch. Harder, H. Jäckel, W. Walter and D. J. Webb: J. Vac. Sci. & Technol. B6 (1988) 692.
9) J. M. Ballingall and C. E. Wood: Appl. Phys. Lett. 41 (1982) 947.
10) W. I. Wang, E. E. Mendez, T. S. Kuan and L. Esaki: Appl. Phys. Lett. 47 (1985) 826.
11) S. Subbanna, H. Kroemer and J. L. Merz: J. Appl. Phys. 59 (1986) 488.
12) M. Shigeta, Y. Okano, H. Seto, H. Katahama, S. Nishine and K. Kobayashi: J. Cryst. Growth 111 (1991) 248.
13) T. Watanabe, T. Yamamoto, P. Vaccaro, H. Ohnishi and K. Fujita: Microelectron. J. 27 (1996) 411.
14) K. Sato, M. R. Fahy and B. A. Joyce: Surf. Sci. 315 (1994) 105; K. Sato, M. R. Fahy and B. A. Joyce: Jpn. J. Appl. Phys. 33 (1994) L905; M. R. Fahy, K. Sato and B. A. Joyce: Appl. Phys. Lett. 64 (1994) 190.
15) M. Fahy, P. Vaccaro, K. Fujita, M. Takahashi, B. A. Joyce and T. Watanabe: Micro-electron. J. (in press); M. R. Fahy, K. Sato, P. Vaccaro, K. Fujita, M. Takahashi, T. Watanabe and B. A. Joyce: Thin Solid Films (in press).
16) T. Yamamoto, M. Inai, T. Takebe and T. Watanabe: J. Vac. Sci. & Technol. A11 (1993) 631.
17) D. R. Lovell, T. Takebe, T. Yamamoto, M. Inai, K. Kobayashi and T. Watanabe: Jpn. J. Appl. Phys. 31 (1992) L1740; D. R. Lovell, T. Yamamoto, M. Inai, T. Takebe and K. Kobayashi: Jpn. J. Appl. Phys. 31 (1992) L924; D. R. Lovell, T. Takebe, T. Yamamoto, M. Inai, K. Kobayashi and T. Watanabe: Jpn. J. Appl. Phys. 32 (1993) 4948.
18) Y. Okano, H. Seto, H. Katahama, S. Nishine, I. Fujimoto and T. Suzuki: Jpn. J. Appl.

Phys. 28 (1989) L151.
19) Y. Kadoya, A. Sato, H. Kano and H. Sakaki: J. Cryst. Growth 111 (1991) 280.
20) L. Pavesi, M. Henini and D. Johnston: App. Phys. Lett. 66 (1995) 2846.
21) Y. Okano, M. Shigeta, H. Seto, H. Katahama, S. Nishine and I. Fujimoto: Jpn. J. Appl. Phys. 29 (1900) L1357.
22) K. Fujita, A. Shinoda, M. Inai, T. Yamamoto, M. Fujii, D. Lovell, T. Takebe and K. Kobayashi: J. Cryst. Growth 127 (1993) 50.
23) A. Shinoda, T. Yamamoto, M. Inai, T. Takebe and T. Watanabe: Jpn. J. Appl. Phys. 32 (1993) L1374.
24) M. Hirai, H. Ohnishi, K. Fujita, P. Vaccaro and T. Watanabe: J. Cryst. Growth 150 (1995) 209; M. Hirai, H. Ohnishi, K. Fujita and T. Watanabe: Jpn. J. Appl. Phys. Lett. 35 (1996) L751.
25) M. Hirai, H. Ohnishi, K. Fujita and T. Watanabe: Appl. Surf. Sci., 82/83 (1994) 23.
26) H. C. Nutt, R. S. Smith, M. Towers, P. K. Rees and D. J. James: J. Appl. Phys. 70 (1991) 821.
27) N. Sakamoto, K. Hirakawa and T. Ikoma: Appl. Phys. Lett. 67 (1995) 1444.
28) K. Fujita, T. Yamamoto, T. Takebe and T. Watanabe: Jpn. J. Appl. Phys. 32 (1993) L978.
29) H. Ohnishi, M. Hirai, T. Yamamoto, K. Fujita and T. Watanabe: J. Cryst. Growth 150 (1995) 231.
30) O. Kumagai, H. Kawai, Y. Mori and K. Kaneko: Appl. Phys. Lett. 45 (1984) 1322.
31) K. Takarabe, Y. Hirano, S. Minomura, K. Matsuda, H. Ohnishi, K. Fujita and T. Watanabe: Phys. Status Solidi b 198 (1966) 187.
32) W. Q. Li and P. K. Bhattacharya: IEEE Electron Device Lett. 13 (1992) 29. W. Q. Li and P. K. Bhattacharya, S. H. Kwok and R. Merlin: J. Appl. Phys. 72 (1992) 3129.
33) K. Fujita and T. Watanabe: Jpn. J. Appl. Phys. 31 (1995) 430.
34) K. Fujita, K. Nitatori, M. Hosoda, T. Egawa, Y. Niwano, T. Jimbo, M. Umeno and T. Watanabe: J. Cryst. Growth 146 (1995) 384.
35) T. Egawa, Y. Niwano, K. Fujita, K. Nitatori, T. Watanabe, T. Jimbo and M. Umeno: Jpn. J. Appl. Phys. 34 (1995) 1270.
36) M. Henini, P. J. Rodgers, P. A. Grump, B. L. Gallagher and G. Hill: J. Cryst. Growth 150 (1995) 451.
37) T. Yamamoto, M. Fujii, T. Takebe, D. Lovell and K. Kobayashi: 18th Int. Symp. GaAs and Related Compounds, Seattle, ed, G. B. Stringfellow (IOP Publishing, Bristol, 1992) p.31.
38) T. Yamamoto, M. Inai, T. Takebe, M. Fujii and K. Kobayashi: J. Cryst. Growth 127 (1993) 865.
39) T. Yamamoto, M. Inai, A. Shinoda, T. Takebe and T. Watanabe: Jpn. J. Appl. Phys. 32 (1993) 3346.
40) K. Nitatori, K. Fujita and T. Watanabe: J. Cryst. Growth 146 (1995) 389.

41) P. Vaccaro, M. Takahashi, K. Fujita and T. Watanabe: J. Cryst. Growth 150 (1995) 503; J. Appl. Phys. 76 (1994) 8037.
42) F. H. Pollak, in T. P. Pearsell (Ed), Strained-Layer Superlattices: Physics, (Academic Press, New York, 1990) ch.2, p17.
43) C. G. Van de Walle: Mater. Res. Soc. Symp. Proc. 102 (1988) 565.
44) D. Sun and E. Towe: Jpn. J. Appl. Phys. 33 (1994) 702.
45) R. Tober and T. Bahder: Appl. Phys. Lett. 63 (1993) 2369.
46) P. Vaccaro, K. Tominaga, M. Hosoda, K. Fujita and T. Watanabe: Jpn. J. Appl. Phys. 34 (1995) 1362.
47) P. Vaccaro, M. Hosoda, K. Fujita and T. Watanabe: Jpn. J. Appl. Phys. 35 (1996) 1292; P. Vaccaro, M. Takahashi, K. Fujita and T. Watanabe: Jpn. J. Appl. Phys., 34 (1995) L13.
48) M. Takahashi, P.Vaccaro, K. Fujita and T. Watanabe: Appl. Phys. Lett., 66 (1995) 93.
49) T. Ohtoshi, T. Kuroda, A. Niwa and S. Tsuji: Appl. Phys. Lett. 65 (1994) 1886.
50) Y. Kajikawa, O. Brandt, K. Kanamoto and N. Tsukada: J. Cryst. Growth 150 (1995) 431.
51) Y. Kaneko, S. Nakagawa, T. Takeuchi, D. E. Mars, N. Yamada and N. Mikoshiba: Electron. Lett. 31 (1995) 805.
52) M. Takahashi, P. Vaccaro, T. Watanabe, T. Mukaihara, F. Koyama and K. Iga: Jpn. J. Appl. Phys. 35 (1996) 6102; M. Takahashi, P. Vaccaro, K. Fujita, T. Watanabe, T. Mukaihara, F. Koyama and K. Iga: IEEE Photon. Technol. Lett. 8 (1996) 737.
53) T. Takebe, M. Fujii, T. Yamamoto, K. Fujita and K. Kobayashi: J. Cryst. Growth 162 (1996) 31; T. Takebe, M. Fujii, T. Yamamoto, K. Fujita and T. Watanabe: J. Vac. Sci. & Technol. B 14 (1996) 2731.
54) T. Takebe, M. Fujii, T. Yamamoto, K. Fujita and K. Kobayashi: J. Cryst. Growth 12 (1993) 937; T. Takebe, M. Fujii, T. Yamamoto, K. Fujita and T. Watanabe: J. Appl. Phys. 81 (1997) 7273.
55) T. Takebe, T. Yamamoto, M. Fujii and K. Kobayashi: J. Electrochem. Soc. 140 (1993) 1169.
56) K. Fujita, H. Ohnishi, M. Hirai, K. Shimada and T. Watanabe: Solid-State Electron. 40 (1996) 633.
57) K. Kobayashi, T. Takebe, T. Yamamoto, M. Fujii, M. Inai and D. Lovell: J. Electron. Mater. 22 (1993) 161; M. Fujii, T. Takebe, T. Yamamoto, M. Inai and K. Kobayashi: Supelatt. and Microstruc. 12 (1992) 168.
58) M. Inai, T. Yamamoto, T. Takebe and T. Watanabe: Jpn. J. Appl. Phys. 32 (1993) L1718.
59) L. Esaki: Phys. Rev. 109 (1958) 603.
60) T. Baba: Jpn. J. Appl. Phys. 31 (1992) L455.
61) T. Uemura and T. Baba: Jpn. J. Appl. Phys. 33 (1994) L207.
62) T. Yamamoto, M. Inai, T. Takebe and T. Watanabe: Jpn. J. Appl. Phys. 32 (1993) L28; M. Inai, T. Yamamoto, M. Fujii, T. Takebe and K. Kobayashi: Jpn. J. Appl. Phys. 32 (1993) 523.

63) T. Yamamoto, M. Inai, M. Hosoda, T. Takebe and T. Watanabe: Jpn. J. Appl. Phys. 32 (1993) 4454.
64) H. Ohnishi, M. Hirai, K. Fujita and T. Watanabe: J. Appl. Phys. 35 (1996) 1168.
65) H. Ohnishi, M. Hirai, K. Fujita and T. Watanabe: Jpn. J. Appl. Phys. 36 (1997) 1853.
66) Y. Nakamura, S. Koshiba, M. Tsuchiya, H. Kano and H. Sakaki: Appl. Phys. Lett. 59 (1991) 700.
67) S. Tsukamoto, Y. Nagamune, M. Nishioka and Y. Arakawa: J. Appl. Phys. 71 (1992) 533.
68) Y. Liu, N. Yamamoto, Y. Nishimoto, N. Kamikubo, S. Shimomura, K. Gamo, K. Murase, N. Sano, A. Adachi, K. Fujita, T. Watanabe and S. Hiyamizu: J. Cryst. Growth 150 (1995) 299.
69) N. Tomita, M. Tanaka, T. Saeki, S. Shimomura, S. Hiyamizu, K. Fujita, T. Watanabe, T. Higuchi, N. Sano and A. Adachi: J. Vac. Sci. & Technol. B14 (1996) 3550.
70) D. Leonard, M. Krishnamurthy, S. Fafard, J. L. Merz and P. M. Petroff: J. Vac. Sci. & Technol. B12 (1994) 1063.
71) J-Y. Marzin, J-M. Gérard, A. Izraël, D. Barrier and G. Bastard: Phys. Rev. Lett. 73 (1994) 716.
72) N. Grandjean and J. Massies: J. Cryst. Growth 134 (1993) 51.
73) E. Tournié and K. H. Ploog: J. Cryst. Growth 135 (1994) 97.
74) K. Mukai, N. Ohtsuka, M. Sugawara and S. Yamazaki: Jpn. J. Appl. Phys. 33 (1994) L1710.
75) J. Oshinowo, M. Nishioka, S. Ishida and Y. Arakawa: Jpn. J. Appl. Phys. 33 (1994) L1634.
76) R. Nötzel, J. Temmyo and T. Tamamura: Appl. Phys. Lett. 64 (1994) 3557.
77) E. Tournié, R. Nötzel and K. H. Ploog: Appl. Phys. Lett. 63 (1993) 3300.
78) P. Vaccaro, M. Hirai, K. Fujita and T. Watanabe: J. Phys. D. 29 (1996) 2221.
79) M. Gurioli, A. Vinattieri, M. Colocci, C. Deparis, J. Massies, G. Neu, A. Bosacchi and S. Franchi: Pys. Rev. B44 (1991) 3115.
80) P. Vaccaro, K. Fujita and T. Watanabe: Jpn. J. Appl. Phys. 36 (1997) 1948.
81) S. Shimomura, A. Wakejima, A. Adachi, Y. Okamoto, N. Sano, K. Murase and S. Hiyamizu: Jpn. J. Appl. Phys. 32 (1993) L1728; Y. Tsuda, S. Shimomura, S. Hiyamizu and N. Sano: J. Cryst. Growth 150 (1995) 415.
82) H. Yamaguchi, M. R. Fahy and B. A. Joyce: Appl. Phys. Lett. 69 (1996) 776.

TABLE I. Etching processes for (111)A GaAs wafers.

Process type	A	B	C	D	E	F
Removed surface oxide layer	Dipping in H_2SO_4:H_2O solution for 1 min rinsing by water and drying by N_2 gas					
Etching process	NH_4OH:H_2O_2:H_2O			H_2SO_4:H_2O_2:H_2O		No etching passed
		2:1:96	2:1:10	5:1:1	5:1:15	
Drying process	Rinsing for 5 min and drying by N_2 gas					
Surface treatments before loading wafers	None	125 °C 30 min Baking in the air	None	None		None
Etching rate (nm/min) for (111)A GaAs		77	541	709	321	

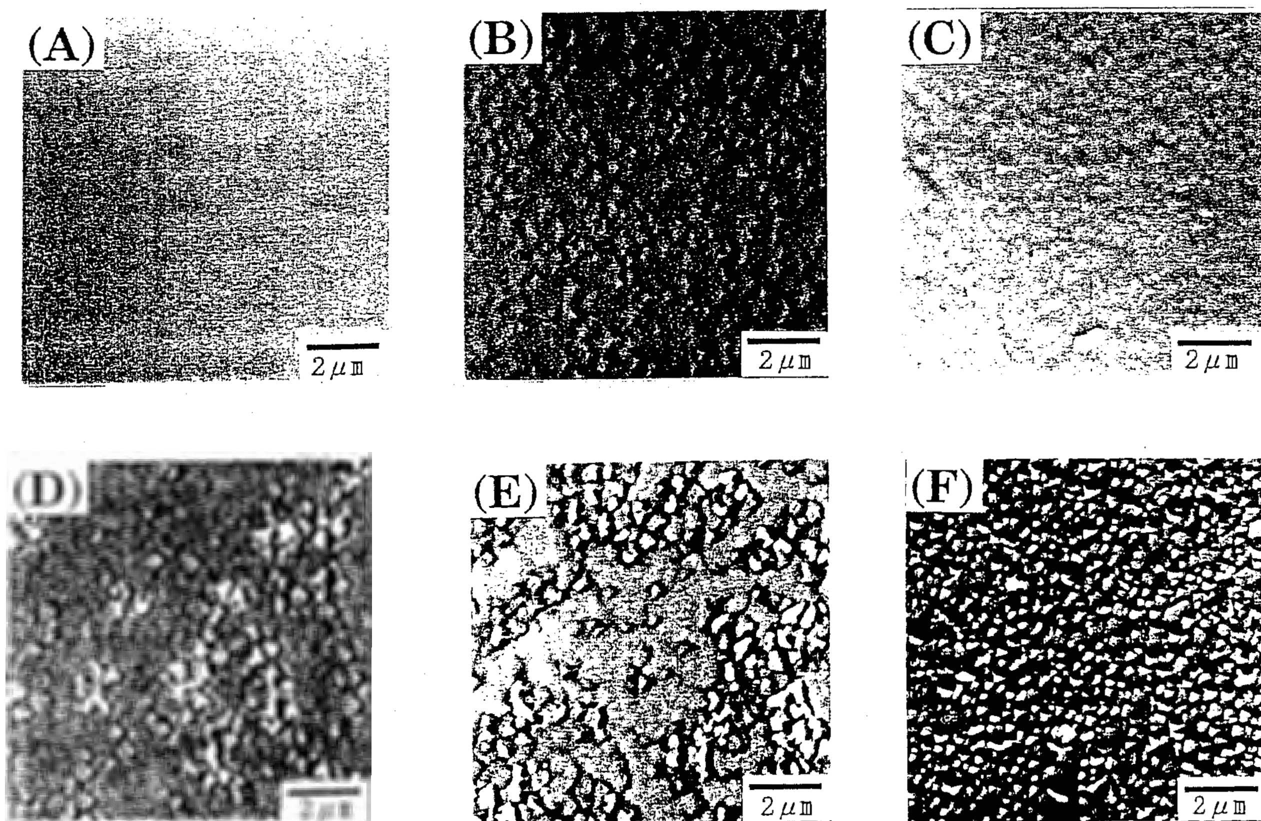

Fig. 1. Etching processes for (111)A wafers and SEM photographs of the surface morphologies of Si-doped GaAs growth layers with a (111)A orientation. The characters (A)-(F) indicate the pregrowth process types described in the table.

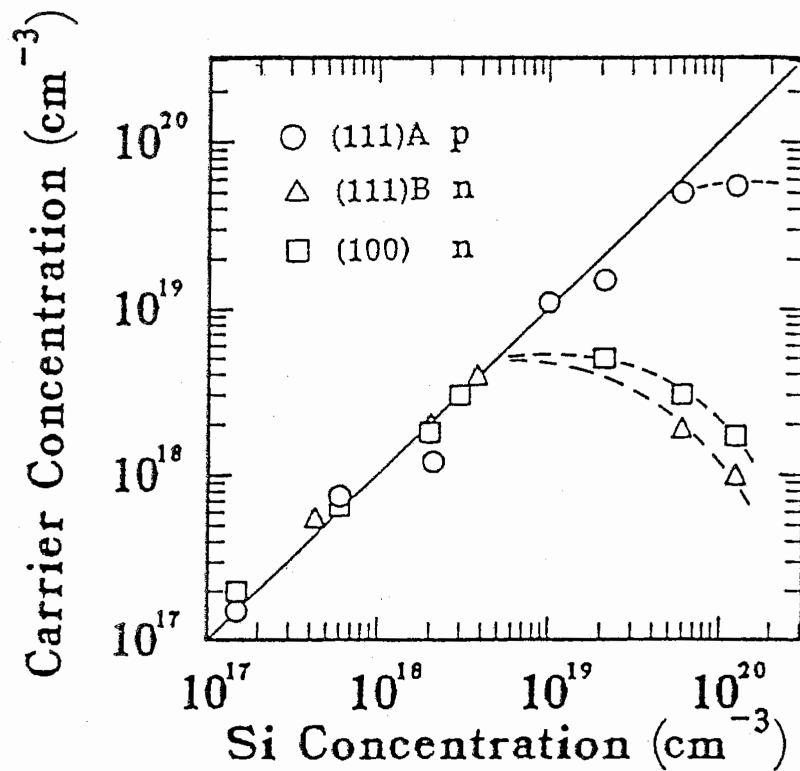

Fig. 2. Free carrier concentrations at room temperature of Si-doped GaAs as a function of the incorporated Si concentration. The circles and squares represent films grown on (111)A and (100) substrates, respectively.

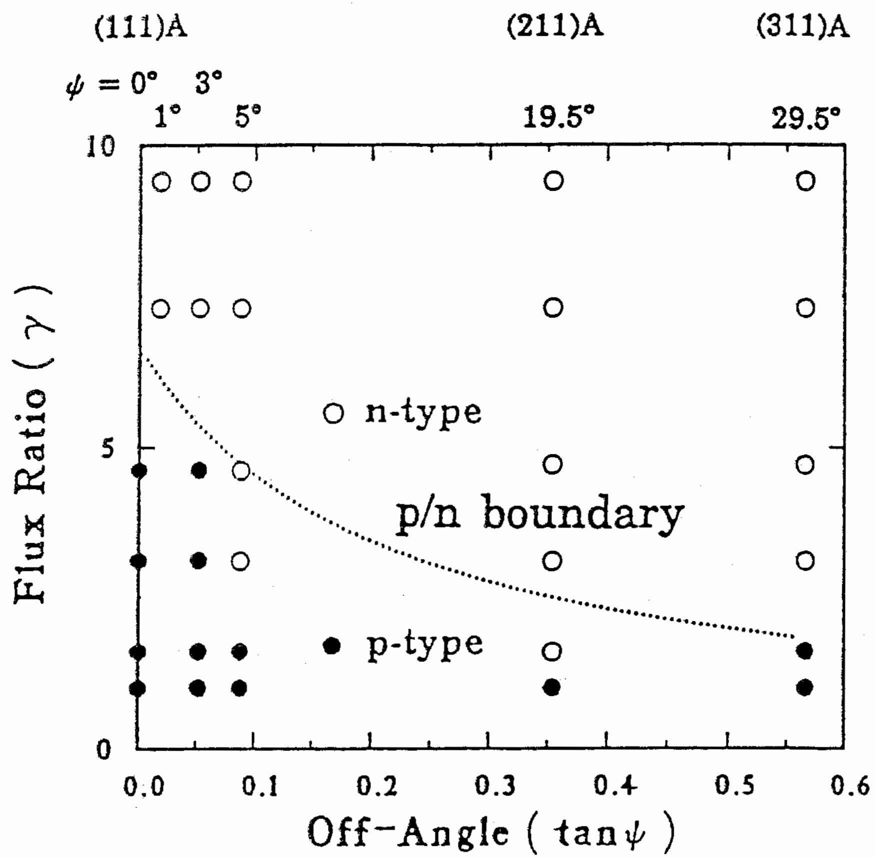

Fig. 3. Conductivity map in plane of tilting angle (φ) and flux ratio (γ).

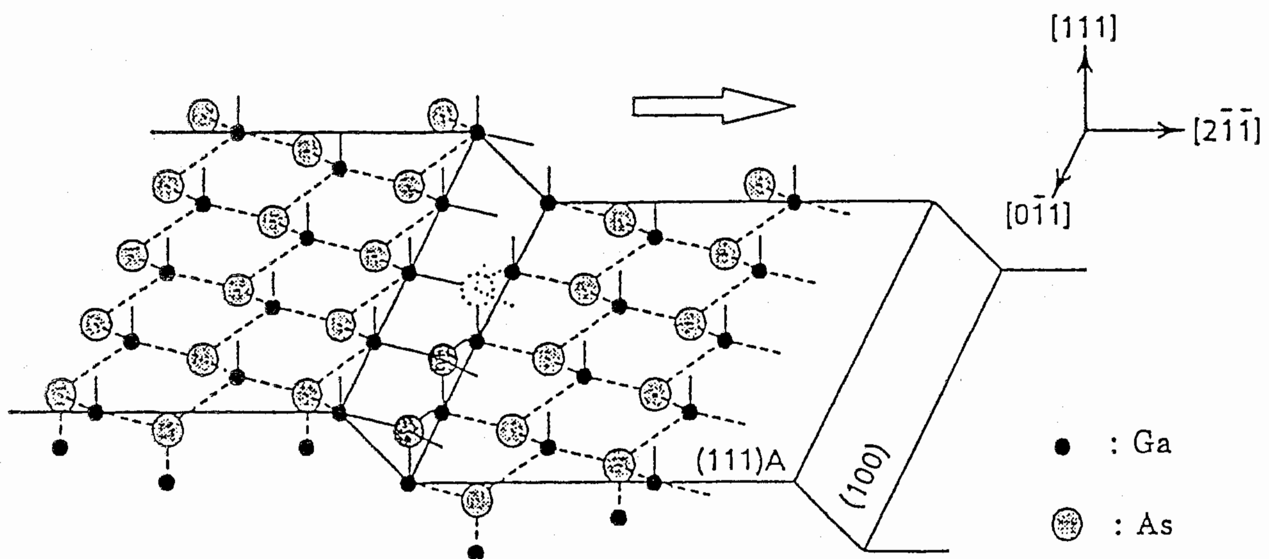

Fig. 4. Crystallographic scheme of an ideal misoriented GaAs(111)A surface, showing different kinds of bonding sites.

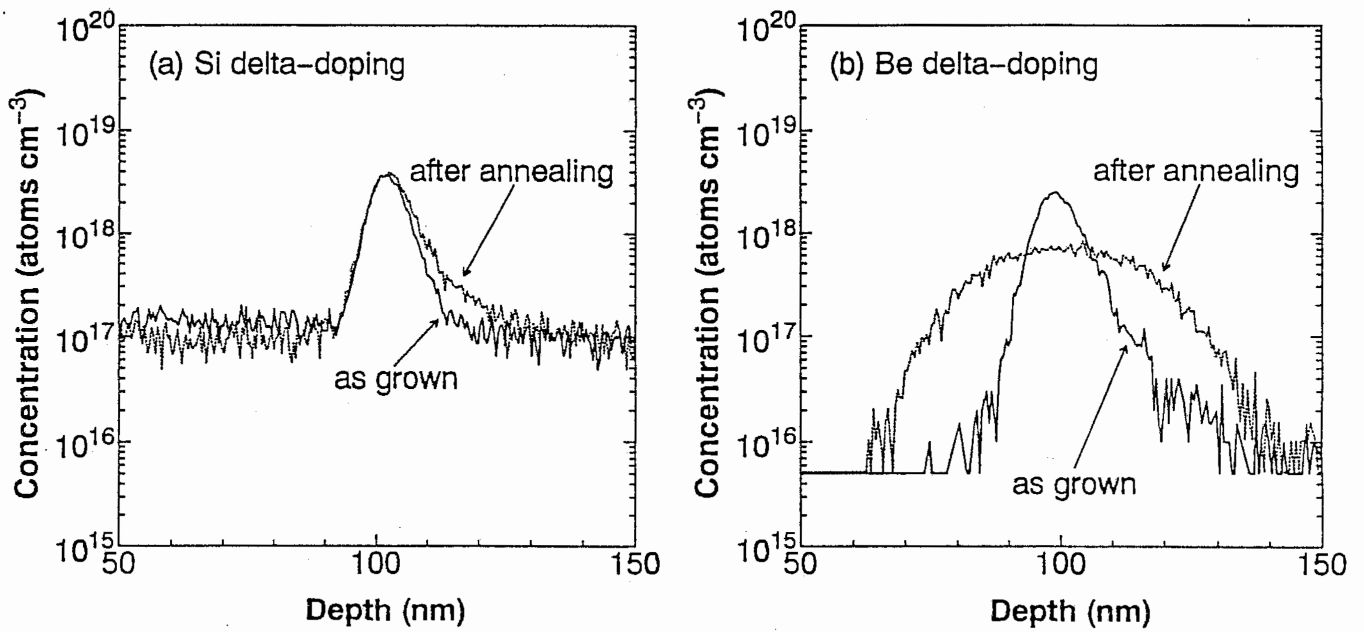

Fig. 5. SIMS depth profiles (a) for Si at a Si delta-doped GaAs layer and (b) for Be at a Be delta-doped GaAs layer. The samples were annealed at 850°C for 30 s.

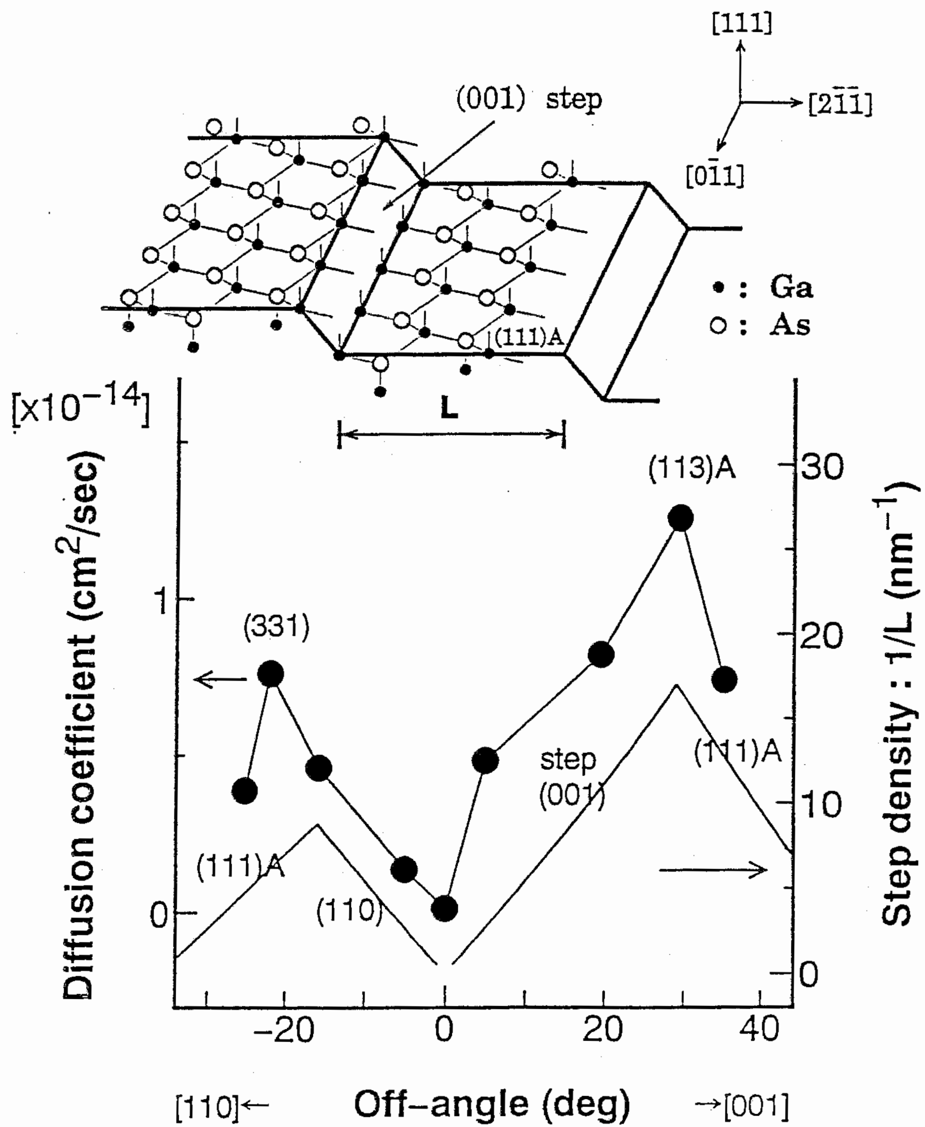

Fig. 6. Diffusion coefficient for Si and step density versus off-angle of a misoriented GaAs(111)A substrate.

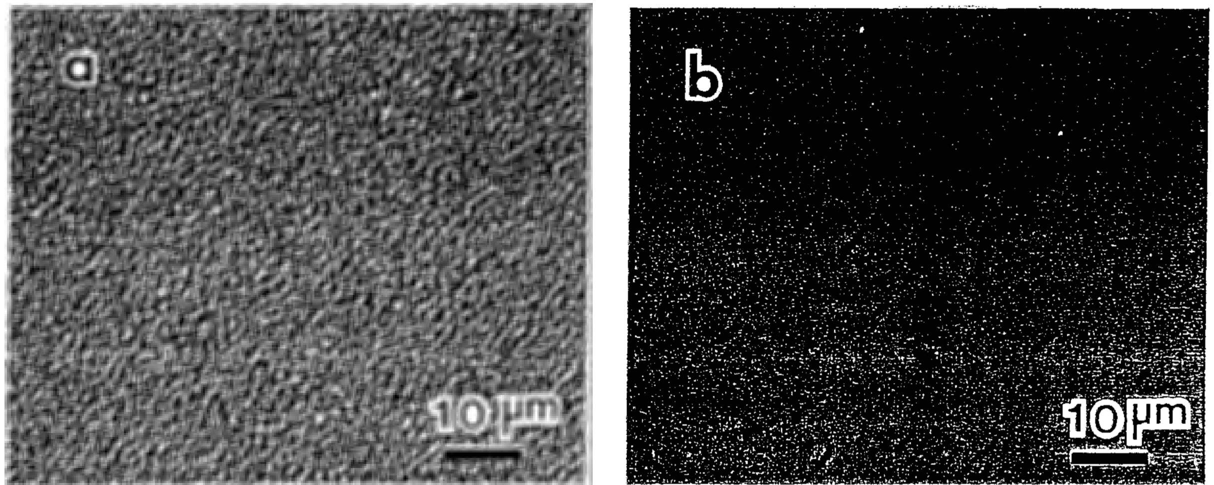

Fig. 7. Surface morphology of AlGaAs layers grown on GaAs(111)A with a flux ratio of 2. The substrate orientation are (a) 3° off and (b) 5° off.

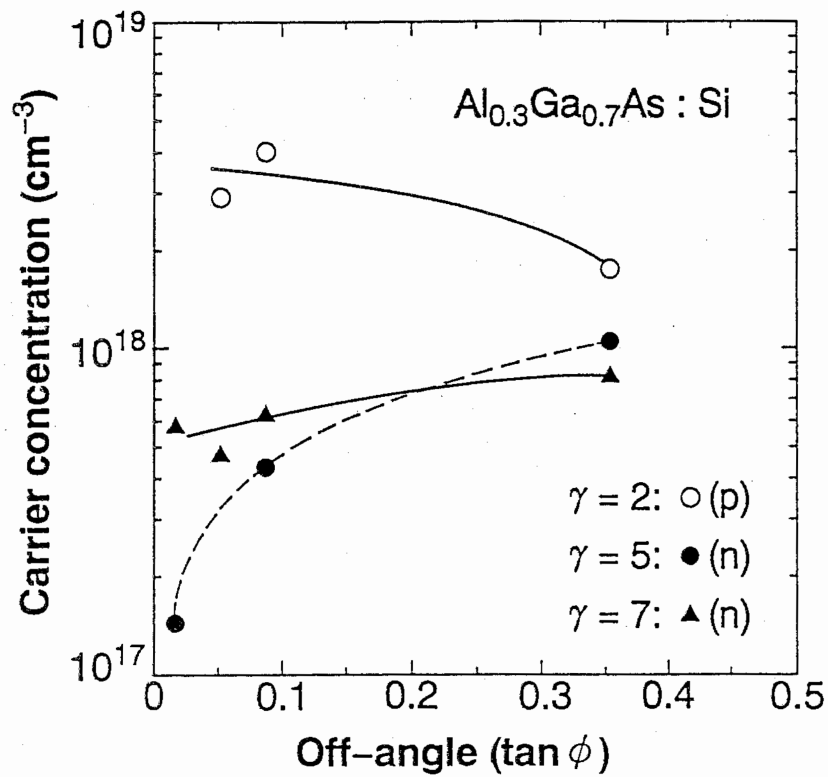

Fig. 8. Dependence of the carrier concentration of Si-doped AlGaAs on the off-angle of substrate orientation.

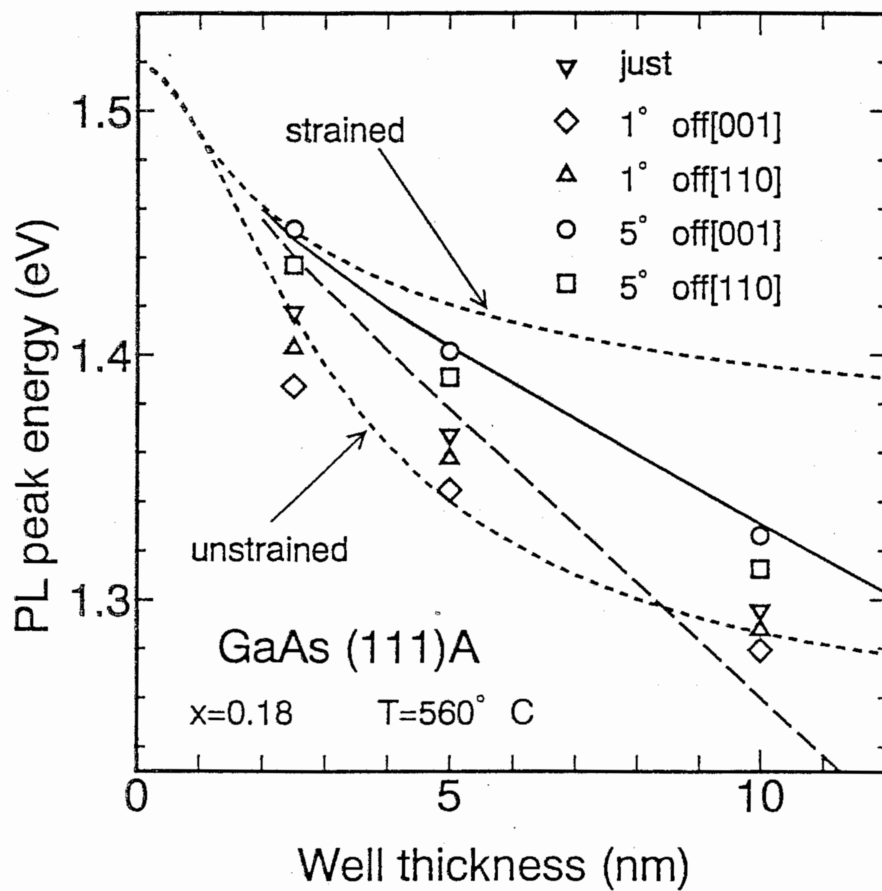

Fig. 9. Photoluminescence peak energy dependence on the well thickness for SQWs grown on GaAs(111)A substrates. The short-dashed lines are the calculated transition energies for strained and relaxed $In_{0.18}Ga_{0.82}As$. The long-dashed line is a calculated result including the theoretical piezoelectric field (E=257 kV/cm). The solid line is a calculated result with a piezoelectric field of E=154 kV/cm to fit the experimental data.

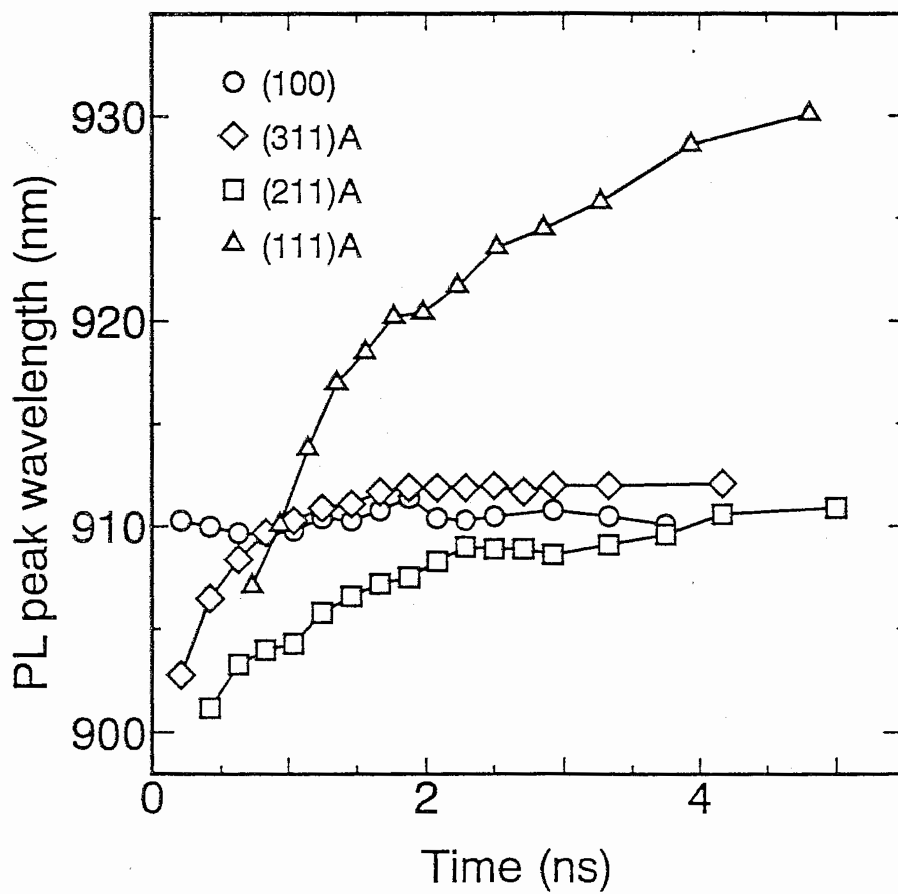

Fig. 10. Time dependence of PL peak wavelength for InGaAs SQWs grown on various substrates. The (111)A sample shows the largest PL peak red-shift because it has the stronger piezoelectric field.

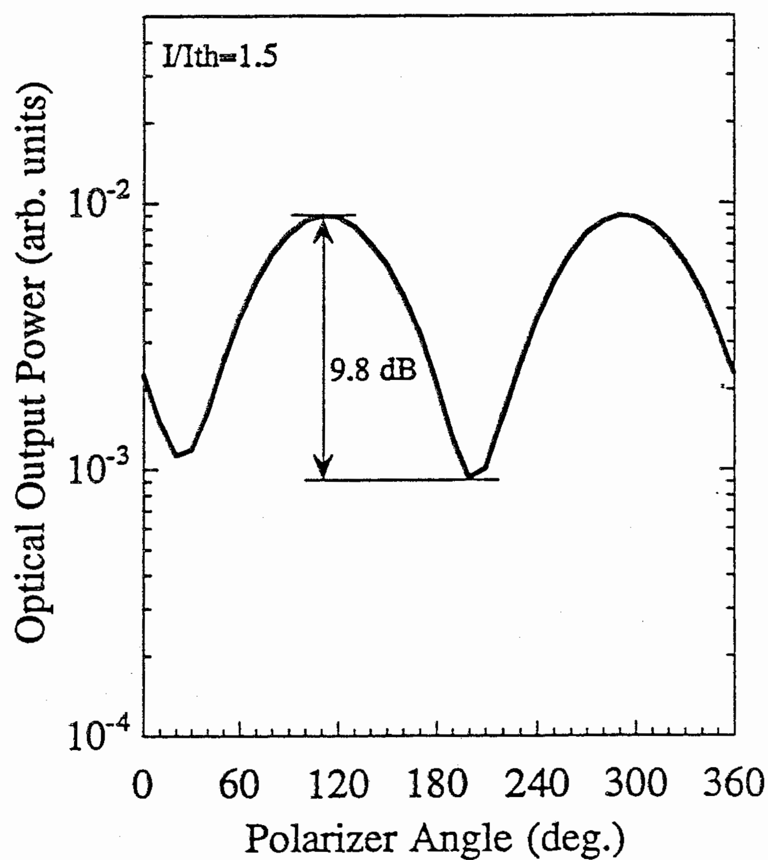

Fig. 11. Light output power versus polarizer angle at 1.5 times the threshold. The extinction ratio between the orthogonal polarization states was 9.8 dB, which corresponds to a net gain difference of 5% between two polarization modes.

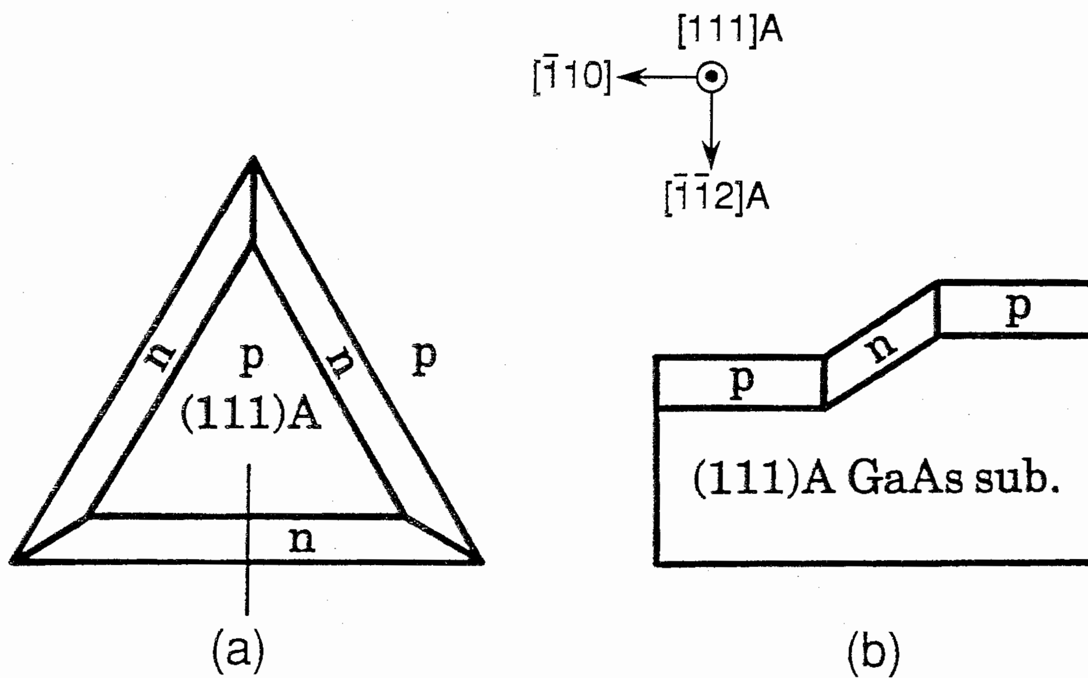

Fig. 12. Schematic illustration of lateral carrier confinement structures on a patterned GaAs(111)A substrate. (a) Top view, and (b) cross-sectional view of the junction along the line indicated in (a).

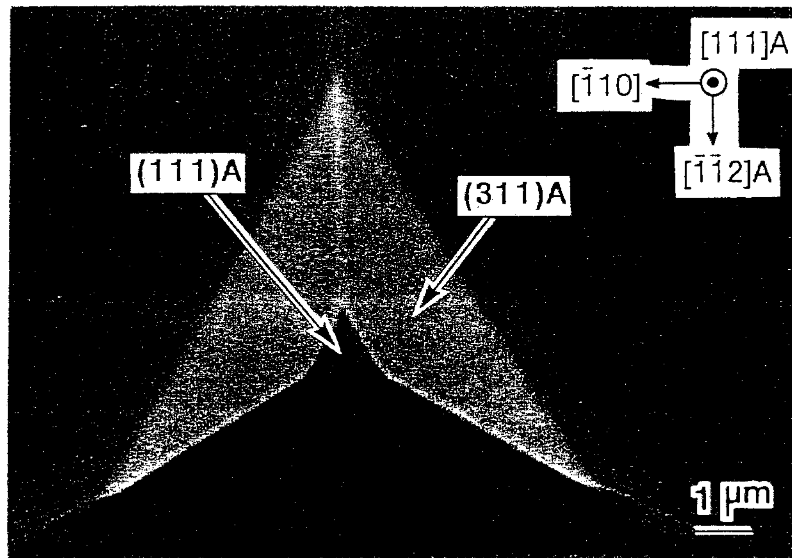

Fig. 13. SEM image of patterned GaAs(111)A with (311)A sidewalls after GaAs growth.

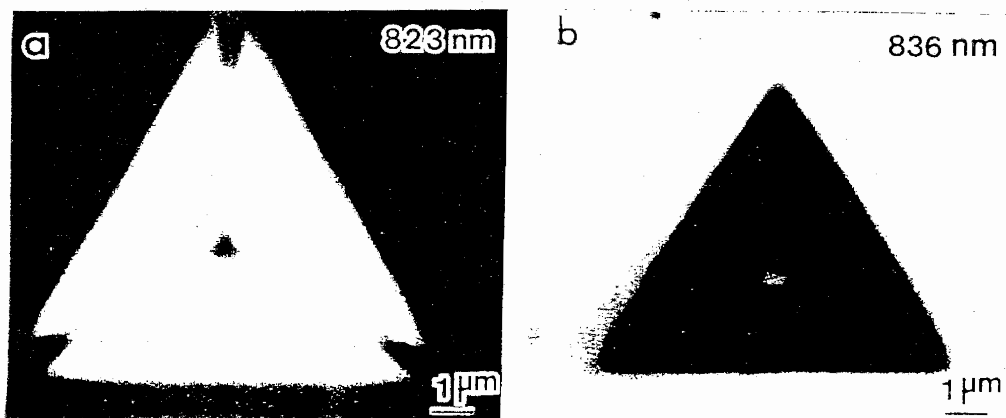

Fig. 14. CL images of a Si-doped GaAs layer on patterned GaAs(111)A. (a) Image taken at the peak wavelength of the (311)A sidewall. (b) Image taken at the wavelength of the upper (111)A region.

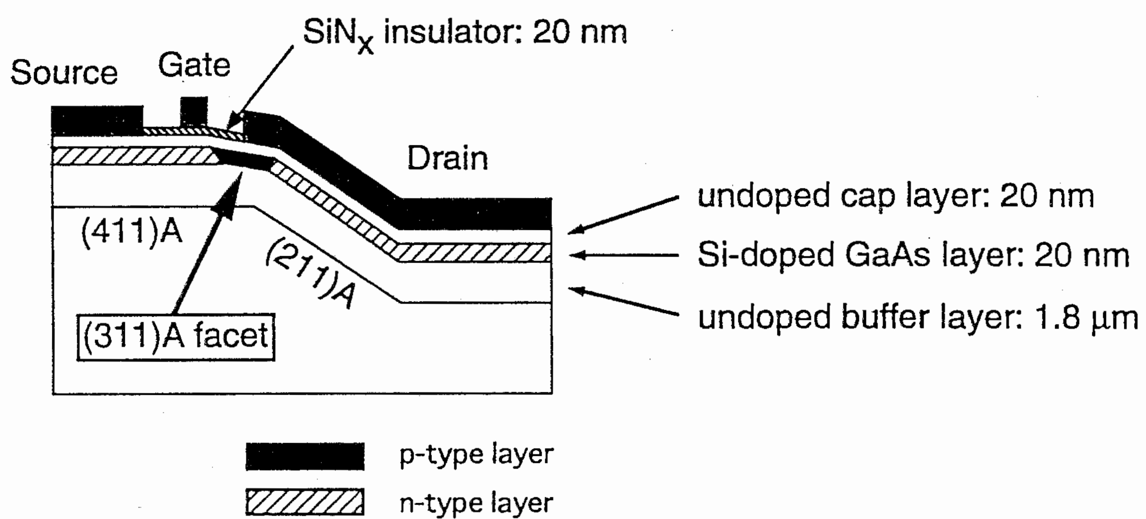

Fig. 15. Schematic cross-sectional view of a lateral tunneling transistor.

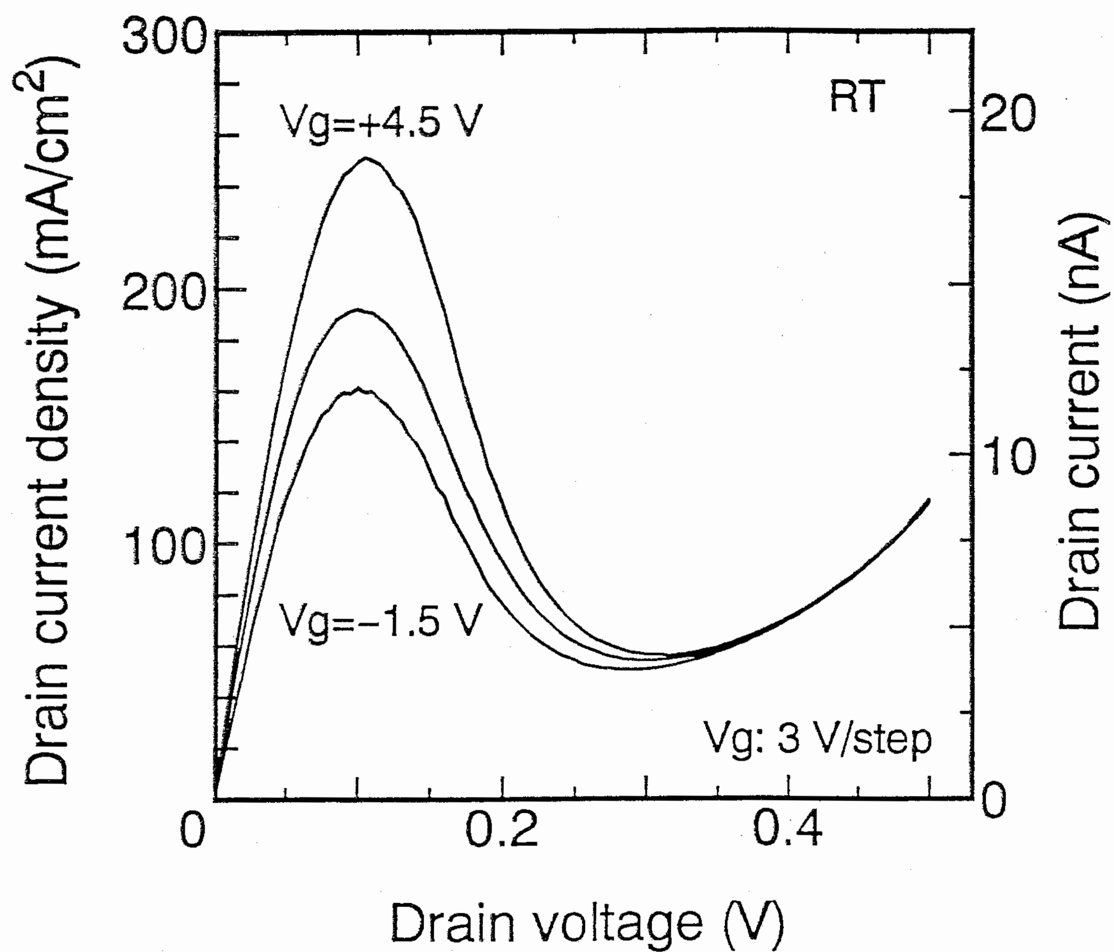

Fig. 16. Drain current-voltage characteristics of a fabricated lateral tunneling transistor at room temperature.The drain voltage is swept from 0.0 to 0.5V with the gate voltage applied in steps of 3.0 V from -1.5 to 4.5 V.

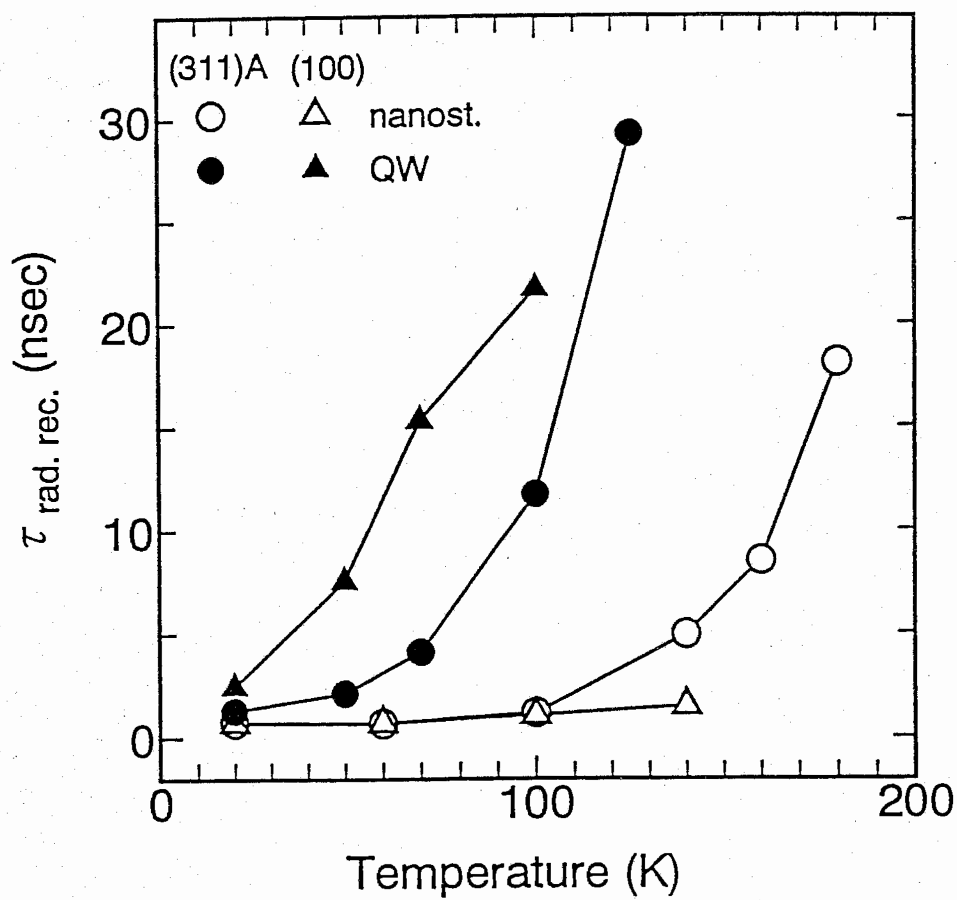

Fig. 17. Radiative recombination time constant dependence on time for nanostructures and conventional quantum wells grown on (311)A and (100) substrates.

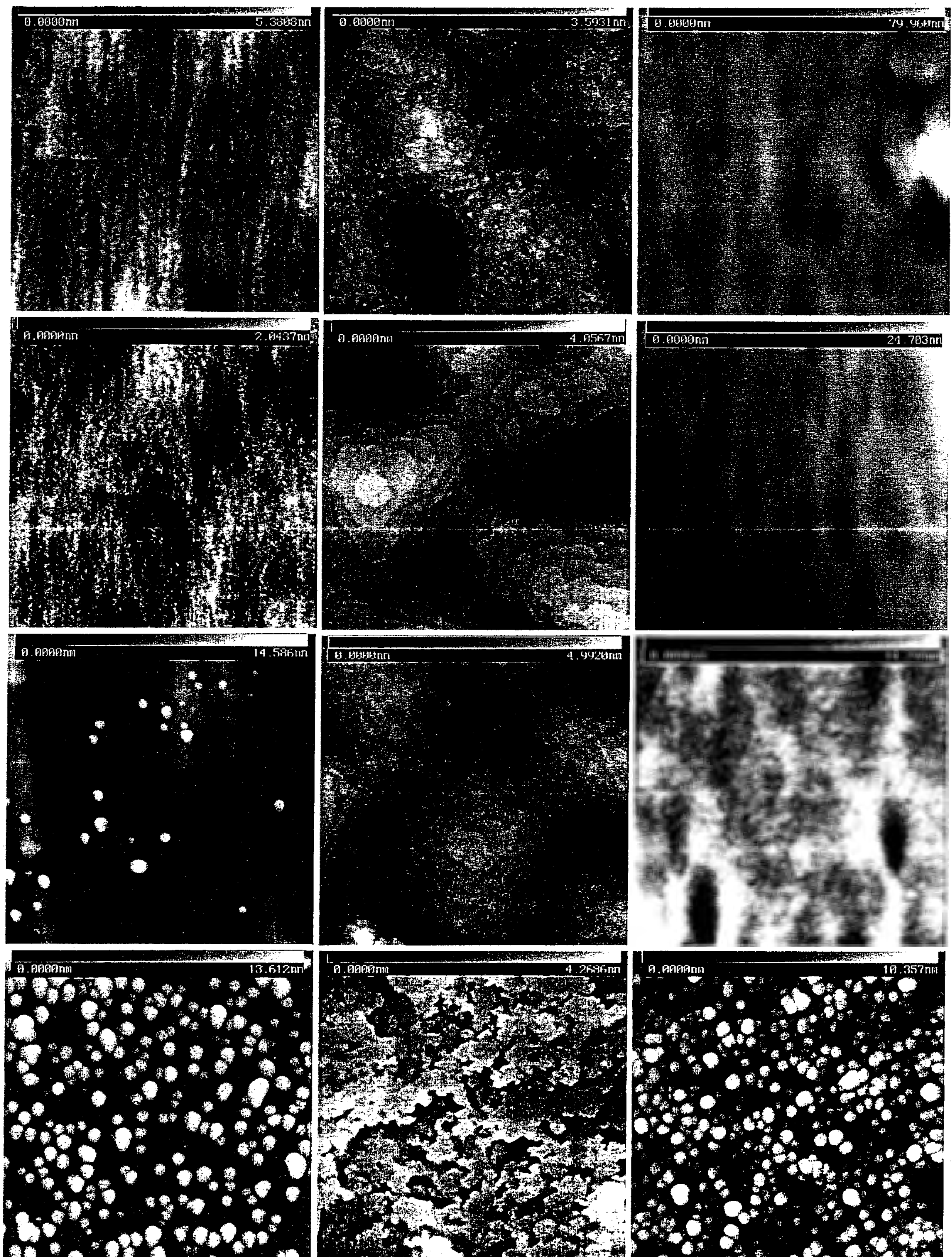

Fig. 18. Morphology of a GaAs buffer layer and surfaces after an amount of InAs equivalent to zero, one, two or three monolayers is deposited on GaAs(411)A,exact (111)A, and 15° off-oriented substrates, observed by AFM. Each micrograph shows an area of 1 μm x 1 μm. The horizontal direction in the micrographs corresponds to the (0$\bar{1}$1) direction, and the vertical direction corresponds to the ($\bar{2}$11) direction for the (111)A substrates and to the ($\bar{2}$44) for the (411)A substrate.